Power Factor Correction Focusing on Magnetic Coupling of Parallel-connected Wires for Inductive Power Transfer System

Keita Furukawa, Keisuke Kusaka, Jun-ichi Itoh
Nagaoka University of Technology
Department of Electrical, Electronics and Information
Nagaoka, Niigata, Japan
archer_FK@stn.nagaokaut.ac.jp, kusaka@vos.nagaokaut.ac.jp, -itoh@vos.nagaokaut.ac.jp

Abstract— **This paper proposes a power factor correction method of a non-resonant IPT system using a four-winding transformer. The proposed technique is applied to the IPT system with a dual active bridge converter to reduce conduction loss and winding loss. When two pairs of the primary-side and the secondary-side wires are connected in parallel, the low coupling coefficient between the wires driven by in-phase voltage corrects the power factor from the viewpoint of the power supply due to the improvement of an equivalent magnetic coupling. The effect of the power factor correction is assessed by experiments with two four-winding transformers, coupling coefficient of which is different from each other. As experimental results, it is confirmed that a maximum efficiency with the lower coupling coefficient between the parallel connected wires is improved by 3.0% in comparison with the system, which has the high coupling coefficient.**

Keywords—wireless power transfer; multi-winding transformer; non-resonant inductive power transfer; dual active bridge

I. INTRODUCTION

In recent years, inductive power transfer (IPT) systems have attracted many researchers as a safety and convenient battery chargers for electrical vehicles (EVs) [1-6]. The IPT systems are able to achieve power transmission without electrical contacts. An increase in a transmission distance of transmission coils causes a reduction of mutual inductance, which results in a low power factor from the view of power supply because the reactive current increases [7]. Large reactive current is one of the factors reducing system efficiency.

In order to correct the power factor, the IPT systems using resonance phenomena have been proposed [1-6][8]. Resonant capacitors are connected in series or parallel to the transmission coils in order to compensate the reactance of the coils by LC resonance [1-6]. Therefore, the resonant IPT systems can achieve unity power factor at the resonance frequency because reactive current is canceled. Considering with actual high-power applications, however, position misalignment of coils or tolerance of resonant component degrades the transmission efficiency because the resonant frequency does not match an operation frequency [1], [6]. In particular, capacitive load increases switching loss of a primary-side inverter because ZVS (zero voltage switching) and ZCS (zero current switching) are not achieved [8].

In order to solve the above-mentioned problems of the resonant IPT system, the non-resonant IPT system utilizing a dual active bridge (DAB) converter has been proposed [9]. In the system, the transmission power is determined by a phase difference between the inverter output voltages of the primary side and the secondary side. This method achieves the power factor correction without resonant capacitors [8]. Besides, ZVS is achieved at all switching devices despite load conditions [9]-[10]. However, high reactive current still leads to the increase in a conduction loss of the switching devices and the winding loss of the transmission coils due to low magnetic coupling [10]. Thus the non-resonant IPT system has to achieve the reduction of the conduction loss and the winding loss when the system is employed to lower-magnetic coupling applications.

This paper proposes a power-factor-correction method for non-resonant IPT systems with a multi-winding transformer as one of the solution to overcome issues of the high conduction loss and winding loss. Two or more wires are connected to the primary core and the secondary core in parallel. From the equivalent circuit of the systems, the weak coupling coefficient k_c between the parallel-connected wires decreases equivalent leakage inductance. Thus a low-k_c transformer reduces the reactive current at the same load.

This paper is organized as follows; first, the theoretical expressions of output power and the power factor is derived. Then, the comparative testing results are showed with a 1.1-kW prototype using two multi-winding transformers which have different coupling k_c: the conventional high-k_c transformer and the proposed low-k_c transformer. As a result, power-factor correction and reduction of input current are achieved in the proposed transformer. Moreover, the maximum system efficiency of the prototype circuit is improved from 87.3% to 90.3% with the proposed transformer.

II. CONVENTIONAL METHODS OF IPT SYSTEMS

A. Conventional Resonant Inductive Power Transfer System

Fig. 1 shows the equivalent circuit of the resonant IPT systems focusing on the AC voltage of fundamental frequency. Resonant capacitors are connected to input and output of the transmission coils in series (S/S type). The input current $\boldsymbol{I_{in}}$ and the output current $\boldsymbol{I_{out}}$ of the system are expressed by (1) and (2) [8].

$$\dot{I}_{in} = \frac{r + R + j\left(\omega L - \frac{1}{\omega C}\right)}{\left\{r + j\left(\omega L - \frac{1}{\omega C}\right)\right\}\left\{r + R + j\left(\omega L - \frac{1}{\omega C}\right)\right\} + (\omega k L)^2}\dot{V}_p \quad (1)$$

$$\dot{I}_{out} = \frac{-j\omega k L}{\left\{r + j\left(\omega L - \frac{1}{\omega C}\right)\right\}\left\{r + R + j\left(\omega L - \frac{1}{\omega C}\right)\right\} + (\omega k L)^2}\dot{V}_p \quad (2)$$

where $\boldsymbol{V_p}$ is the input voltage, L is the self-inductance of the transmission coils, r is the equivalent series resistance, C is the capacitance of the resonant capacitors, R is the load resistance and k is the coupling coefficient between the transmission coils.

The value C is designed to cancel the reactance of the self-inductance of the transmission coils. The resonance angular frequency ω_0 is decided by (3) [8].

$$\omega_0 = \frac{1}{\sqrt{LC}} \quad (3)$$

The operation frequency f_{sw} of the inverter is generally designed same or a little larger than the resonance frequency $\omega_0/(2\pi)$ to reduce switching loss with zero-voltage-switching (ZVS) or zero-current-switching (ZCS). However, the error of ω_0 due to position misalignment of coils or tolerance of the resonant components causes the degradation of the system efficiency and the output power. In particular, the inverters operate neither ZCS nor ZVS with a capacitive load. In addition, low power factor is caused by the increased reactance.

B. Non-resonant Inductive Power Transfer System Applied to Dual Active Bridge

Fig. 2 shows the non-resonant IPT system utilizing the DAB converter [9]. The single-phase full-bridge inverters are employed at both the primary side and the secondary side of the transmission coils.

Fig. 3 shows the operation principle of the non-resonant IPT system. Not only the primary inverter but also the secondary inverter supply AC voltage v_p and v_s to the transmission coils. Note that the inverters output two-level voltage and the frequency of the output voltage is same. Transmission power P is presented by

$$P = \frac{k V_{in} V_{out}}{2\pi f_{sw} L (1-k)^2}\delta\left(1 - \frac{|\delta|}{\pi}\right) \quad (4),$$

where V_{in} and V_{out} are the input and output DC voltage, L is the self-inductance of the transmission coils, and δ is the lagging phase difference between v_s and v_p.

The transmission power of the non-resonant IPT system is controlled by adjusting the lagging phase difference [9]. If δ is positive, the power flow is primary side to secondary side. On the other hand, when δ is negative, the power flow is secondary side to primary side. Thus the non-resonant IPT system achieves not only the control of the transmission power, but also the bi-directional operation without additional compensation circuits [9].

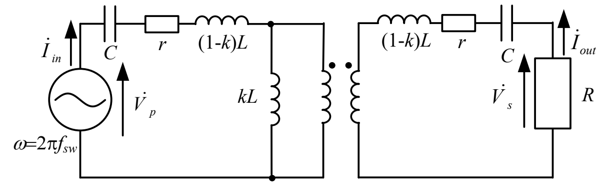

Fig. 1. Equivalent circuit of a S/S resonant IPT system. The self-inductance and the equivalent series resistances r in each the primary side and secondary side are same value for simplify.

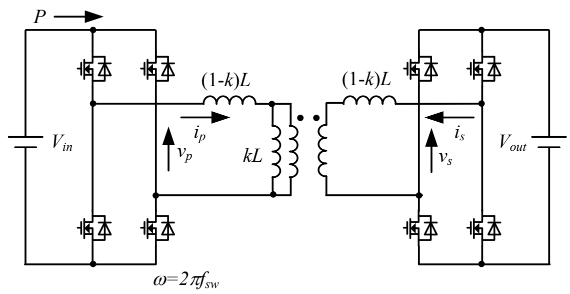

Fig. 2. Non-resonant IPT system applied dual active bridge.

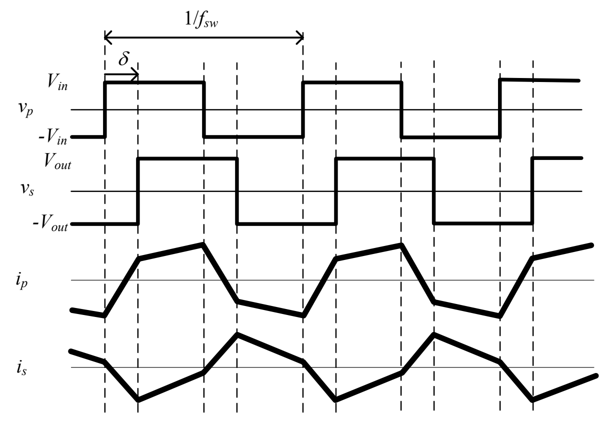

Fig. 3. Voltage and current waveforms of non-resonant IPT system utilized dual active bridge. The inverters are operated as two-level inverter. Polarities of the voltage and directions of the current is defined in Fig. 2.

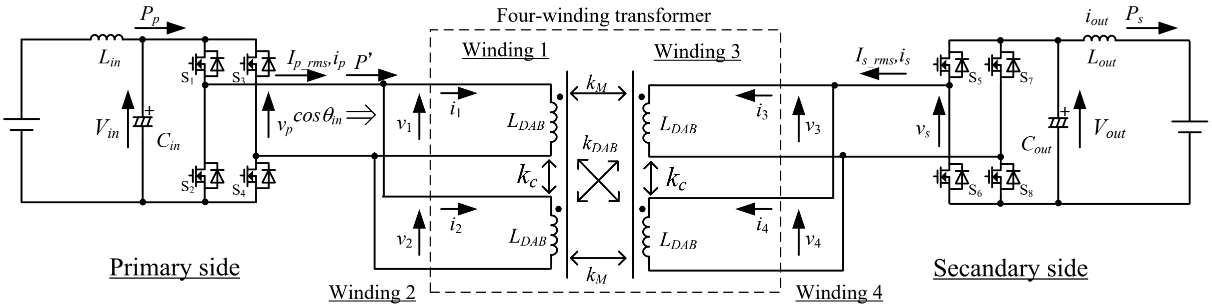

Fig. 4. Circuit configuration of proposed IPT system using four-winding transformer. The cores of the four-winding transformer is shared in each the primary side and the secondary side. The output power P_{out} is defined as lower value of $|P_p|$ or $|P_s|$.

The total power factor from the view point of the inverter is always lower than 1, because the excitation current flows for the small mutual inductance regardless of δ [9] [10]. In particular, when the coupling coefficient k is significantly low (k = 0.01–0.2), the power factor is greatly decreased because of the large excitation current. The increase in the excitation current causes large conduction loss and copper loss. Therefore, it is important to keep the coupling coefficient as high as possible. In the next section, the proposed power-factor-correction method with a four-winding transformer is described.

III. Proposed Circuit Configuration

A. System Configuration

Fig. 4 shows the system configuration of the proposed system. The difference of the proposed system compared with the conventional non-resonant IPT system (Fig. 2) is that the four-winding transformer is introduced as the transmission coils. Two primary side wires are wound onto one shared primary core. The same procedure is carried out at the secondary side. Through this winding structure, the windings on each side are magnetically coupled with the coupling coefficient k_c.

Considering the reduction of power loss in the converter, the multiple single-phase full-bridge inverters should be connected to the each winding. Besides, each of the primary-side inverters and the secondary-side inverters is driven in phase to avoid cross currents. However, only one DAB converter drives the four-winding transformer in this experiment for the simplicity. A parallel connection of the full-bridge inverter is more effective to decrease the conduction loss of MOSFETs because the current is divided into each converter. In next section, a method of increasing an equivalent magnetic coupling between the primary side and the secondary side is discussed.

B. Analysis of Four-winding Transformers

Fig. 5 shows the equivalent circuit of the four-winding transformer [11]. Terminal voltages of windings m (m = 1, 2, 3, 4) contain not only an induced electromotive force from the current flowing through the winding m, but also the sum of the induced voltages from the currents flowing in the other windings. Consequently, the magnetic coupling among four windings has to be considered. The relationship between the input voltage v_m and the input current i_m of the winding m is expressed by using a four-order inductance matrix $\boldsymbol{L_{Trans}}$ as shown in

$$\begin{bmatrix} v_1 \\ v_2 \\ v_3 \\ v_4 \end{bmatrix} = \boldsymbol{L_{Trans}} \frac{d}{dt} \begin{bmatrix} i_1 \\ i_2 \\ i_3 \\ i_4 \end{bmatrix} = \begin{bmatrix} L_{11} & L_{12} & L_{13} & L_{14} \\ L_{21} & L_{22} & L_{23} & L_{24} \\ L_{31} & L_{32} & L_{33} & L_{34} \\ L_{41} & L_{42} & L_{43} & L_{44} \end{bmatrix} \frac{d}{dt} \begin{bmatrix} i_1 \\ i_2 \\ i_3 \\ i_4 \end{bmatrix}$$

$$= \begin{bmatrix} L_{11} & k_{12}\sqrt{L_{11}L_{22}} & k_{13}\sqrt{L_{11}L_{33}} & k_{14}\sqrt{L_{11}L_{44}} \\ k_{21}\sqrt{L_{11}L_{22}} & L_{22} & k_{23}\sqrt{L_{22}L_{33}} & k_{24}\sqrt{L_{22}L_{44}} \\ k_{31}\sqrt{L_{11}L_{33}} & k_{32}\sqrt{L_{22}L_{33}} & L_{33} & k_{34}\sqrt{L_{33}L_{44}} \\ k_{41}\sqrt{L_{11}L_{44}} & k_{42}\sqrt{L_{22}L_{44}} & k_{43}\sqrt{L_{33}L_{44}} & L_{44} \end{bmatrix} \frac{d}{dt} \begin{bmatrix} i_1 \\ i_2 \\ i_3 \\ i_4 \end{bmatrix} \quad \text{(5)},$$

where L_{mm} is the self-inductance of the winding m, and L_{mn} ($m \neq n$, n = 1, 2, 3, 4) is the mutual inductance between the winding m and the winding n. The matrix elements of L_{mn} and L_{nm} at a specific combination of m and n have the same value. Besides, the coupling coefficient k_{mn} of two windings is defined by

$$k_{mn} = \frac{L_{mn}}{\sqrt{L_{mm}L_{nn}}} \quad \text{(6)}.$$

The parameters in Fig. 5 are presented by (7) and (8) [11].

$$\begin{bmatrix} -\frac{1}{Le_{11}} & -\frac{1}{Le_{12}} & -\frac{1}{Le_{13}} & -\frac{1}{Le_{14}} \\ -\frac{1}{Le_{21}} & -\frac{1}{Le_{22}} & -\frac{1}{Le_{23}} & -\frac{1}{Le_{24}} \\ -\frac{1}{Le_{31}} & -\frac{1}{Le_{32}} & -\frac{1}{Le_{33}} & -\frac{1}{Le_{34}} \\ -\frac{1}{Le_{41}} & -\frac{1}{Le_{42}} & -\frac{1}{Le_{43}} & -\frac{1}{Le_{44}} \end{bmatrix} = \boldsymbol{L_{Trans}}^{-1} \quad \text{(7)}$$

$$\begin{bmatrix} \frac{1}{Le_{10}} \\ \frac{1}{Le_{20}} \\ \frac{1}{Le_{30}} \\ \frac{1}{Le_{40}} \end{bmatrix} = -\sum_{n=1}^{4} \begin{bmatrix} \frac{1}{Le_{1n}} \\ \frac{1}{Le_{2n}} \\ \frac{1}{Le_{3n}} \\ \frac{1}{Le_{4n}} \end{bmatrix} \quad \text{(8)}$$

Next, restriction and relationship are given by the symmetry of the circuit. The first one is that the self-inductances of all windings must have the same value L_{DAB}. The second one is that the coupling coefficients of k_M, k_{DAB} and k_c are defined as shown in Fig. 4. Then the relationship of the voltage and the current is expressed by (9).

$$\begin{bmatrix} v_1 \\ v_2 \\ v_3 \\ v_4 \end{bmatrix} = L_{DAB} \begin{bmatrix} 1 & k_c & k_M & k_{DAB} \\ k_c & 1 & k_{DAB} & k_M \\ k_M & k_{DAB} & 1 & k_c \\ k_{DAB} & k_M & k_c & 1 \end{bmatrix} \frac{d}{dt} \begin{bmatrix} i_1 \\ i_2 \\ i_3 \\ i_4 \end{bmatrix} \text{ .... (9)}$$

The inductance values in Fig. 5 are presented by (10)-(13)

$$Le_{12} = Le_{34} = \frac{L_{DAB} f(k_c, k_{DAB}, k_M)}{-2k_M k_{DAB} + k_c(1 - k_c^2 + k_{DAB}^2 + k_M^2)} \text{ ...(10),}$$

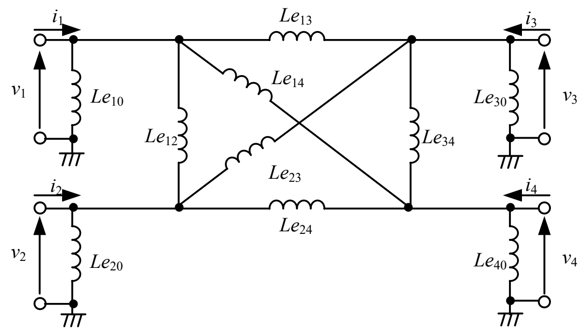

Fig. 5. Equivalent circuit of four-winding transformer. This circuit is extended from the π-type equivalent circuit for two-port network.

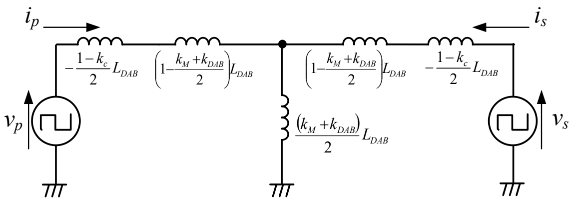

Fig. 6. Equivalent circuit of proposed system. The four-winding transformer is shown as the two-winding transformer. In addition, the two-level full-bridge inverters are shown as the square-wave voltage sources.

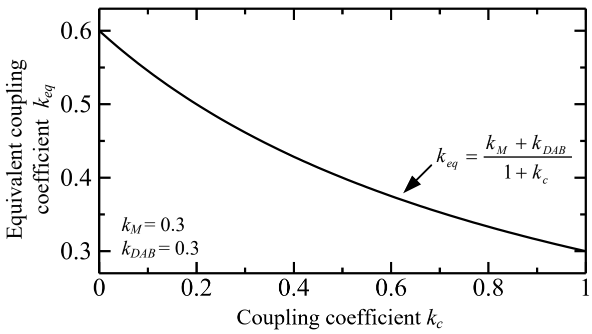

Fig.7. Relationship of equivalent coupling coefficient versus coupling coefficient k_c. Only k_c value is changed from 1 to 0. In order to verify the effect of reducing k_c, k_M and k_{DAB} are fixed value.

$$Le_{13} = Le_{24} = \frac{L_{DAB} f(k_c, k_{DAB}, k_M)}{-2k_c k_{DAB} + k_M(1 + k_c^2 + k_{DAB}^2 - k_M^2)} \text{ ... (11),}$$

$$Le_{14} = Le_{23} = \frac{L_{DAB} f(k_c, k_{DAB}, k_M)}{-2k_M k_c + k_{DAB}(k_M^2 + k_c^2 - k_{DAB}^2 + 1)} \text{ ... (12),}$$

$$Le_{10} = Le_{20} = Le_{30} = Le_{40} = L_{DAB}(1 + k_M + k_c + k_{DAB}) \text{ .. (13),}$$

where the function $f(k_c, k_M, k_{DAB})$ is expressed by (14).

$$f(k_c, k_{DAB}, k_M) = \{(1-k_c)^2 - (k_M - k_{DAB})^2\}\{(1+k_c)^2 - (k_M + k_{DAB})^2\}$$
$$\text{..(14)}$$

When the windings are connected in parallel in each the primary side and the secondary side, the relationship of the voltage and the current is shown in (15) and (16)

$$\begin{bmatrix} i_p \\ i_s \end{bmatrix} = \frac{2\begin{bmatrix} 1+k_c & k_M + k_{DAB} \\ k_M + k_{DAB} & 1+k_c \end{bmatrix}\begin{bmatrix} \int v_p dt \\ \int v_s dt \end{bmatrix}}{L_{DAB}\{(1+k_c)^2 - (k_M + k_{DAB})^2\}} \text{ .... (15),}$$

$$\begin{bmatrix} v_p \\ v_s \end{bmatrix} = L_{DAB} \begin{bmatrix} \frac{1+k_c}{2} & \frac{k_M + k_{DAB}}{2} \\ \frac{k_M + k_{DAB}}{2} & \frac{1+k_c}{2} \end{bmatrix} \frac{d}{dt} \begin{bmatrix} i_p \\ i_s \end{bmatrix} \text{ .... (16),}$$

where v_p is the input voltage of the primary side, v_s is the input voltage of the secondary side, i_p is the equivalent input current of the primary side and i_s is the equivalent input current of the secondary side.

Moreover, the equivalent self-inductance L_p of the primary side, the equivalent self-inductance L_s of the secondary side and the equivalent mutual inductance M are expressed as in (17) and (18).

$$L_p = L_s = \frac{1+k_c}{2} L_{DAB} \text{ .... (17)}$$

$$M = \frac{k_M + k_{DAB}}{2} L_{DAB} \text{ .... (18)}$$

These equivalent values of L_p, L_s and M are useful to analyze the four-winding transformer as a two-winding transformer.

Fig. 6 shows the equivalent circuit of the proposed system. The negative inductance $-L_{DAB}(1-k_c)/2$ is connected in series to the two-winding transformer, the coupling coefficient of which is $(k_M+k_{DAB})/2$. Therefore, the low k_c is effective to reduce the leakage inductance. The equivalent coupling coefficient k_{eq} of the equivalent circuit is presented by (19).

$$k_{eq} = \frac{M}{\sqrt{L_p L_s}} = \frac{k_M + k_{DAB}}{1+k_c} \text{ .... (19)}$$

Fig. 7 shows the relationship of k_{eq} versus k_c. Both of k_M and k_{DAB} are fixed values. The equivalent coupling coefficient k_{eq} is clearly improved with decreasing k_c.

The reason why k_{eq} is increased with the decrease in k_c such as (19) and Fig. 7, is reduction of L_p and L_s from (17) and (18). Generally, combined inductance of wounding in parallel is lower than self-inductance of each winding because. Besides, the combined inductance is much lower when the magnetic coupling of the windings is smaller. Whereas, the value of M is decided despite k_c in the system. In consequence, k_{eq}, which corresponds to ratio of M versus the geometric mean of L_p and L_s is improved.

C. Transmission Power and Power Factor of Proposed System

In this section, the transmission power P' and the power factor of the inverter output are formulated from the equivalent circuit shown in Fig. 6. Moreover, the relationship of the power factor and the coupling coefficient k_c is discussed in detail. From (4), (17) and (19), P' is given by (20) with substituting L_p and k_{eq} for L and k.

$$P' = \frac{2V_{in}V_{out}\left(k_M + k_{DAB}\right)}{\omega L_{DAB}\left\{(1+k_c)^2 - \left(k_M + k_{DAB}\right)^2\right\}}\delta\left(1 - \frac{|\delta|}{\pi}\right) \quad \text{......(20)}$$

RMS values I_{p_rms} and I_{s_rms} of i_p and i_s are shown in (21) and (22).

$$I_{p\_rms} = \sqrt{f_{sw}\int_0^{\frac{1}{f_{sw}}} i_p{}^2 dt}$$
$$= \frac{\sqrt{\pi^3\left\{(1+k_c)V_{in} - \left(k_M + k_{DAB}\right)V_{out}\right\}^2 - 4(1+k_c)\left(k_M + k_{DAB}\right)V_{in}V_{out}\left(2|\delta| - 3\pi\right)\delta^2}}{\omega L_{DAB}\sqrt{3\pi}\left\{(1+k_c)^2 - \left(k_M + k_{DAB}\right)^2\right\}} \quad \text{......(21)}$$

$$I_{s\_rms} = \sqrt{f_{sw}\int_0^{\frac{1}{f_{sw}}} i_s{}^2 dt}$$
$$= \frac{\sqrt{\pi^3\left\{(1+k_c)V_{out} - \left(k_M + k_{DAB}\right)V_{in}\right\}^2 - 4(1+k_c)\left(k_M + k_{DAB}\right)V_{in}V_{out}\left(2|\delta| - 3\pi\right)\delta^2}}{\omega L_{DAB}\sqrt{3\pi}\left\{(1+k_c)^2 - \left(k_M + k_{DAB}\right)^2\right\}} \quad \text{......(22)}$$

When the input DC voltage V_{in} is as same as the output DC voltage V_{out}, the power factor cos θ_{in} from the view point of the output of the primary-side inverter is given by (23).

$$\cos\theta_{in} = \frac{|P'|}{V_{in}I_{p\_rms}}$$
$$= \frac{\sqrt{12\pi}\left(k_M + k_{DAB}\right)|\delta|\left(1 - \frac{|\delta|}{\pi}\right)}{\sqrt{\pi^3\left\{(1+k_c) - \left(k_M + k_{DAB}\right)\right\}^2 + 4(1+k_c)\left(k_M + k_{DAB}\right)\left(3\pi - 2|\delta|\right)\delta^2}} \quad \text{......(23)}$$

Fig. 8 shows theoretical curves of cos θ_{in} with the coupling $0 < k_c < 1$. Note that k_M and k_{DAB} are designed to be 0.3 for IPT systems. Lower k_c (higher k_{eq}) makes the systems higher power factor cos θ_{in} over entire load range. Fig. 6 and Fig. 7 also show that lower k_c reduces the equivalent leakage inductance coming from the four-winding transformer. Thus k_c value should be small to improve cos θ_{in}.

IV. Experimental Results

A. Test Conditions

The proposed improvement method on the magnetic coupling is experimentally verified. The test is carried out with the system configuration shown in Fig. 4. Table I shows the test conditions and parameters of the elements. Note that input and output voltage is 280 V, and the rated power is 1.1 kW.

Fig. 9 shows the pictures of the two four-winding transformers, which are used for the tests. The rectangular cores are made of 21 ferrite plates (TDK, B67345B4X87). Two four-winding transformers have the same size of cores and the same distance between cores for a fair comparison. The parallel-connected windings on the conventional transformer are wound close to each other in order to increase k_c value. Whereas, the parallel-connected windings on the proposed transformer are separately wound on the outside of coils and closely wound at the center of the coils in order to reduce k_c value without decreasing k_M and k_{DAB}. The coupling coefficients k_c, k_M and k_{DAB} are determined by the dispositions of the wires. The self-inductance L_{DAB} is adjusted by turns of coils and given by (24) using maximum power P_{max}.

$$L_{DAB} = \frac{\pi}{2}\frac{V_{in}V_{out}\left(k_M + k_{DAB}\right)}{\omega P_{\max}\left\{(1+k_c)^2 - \left(k_M + k_{DAB}\right)^2\right\}} \quad \text{................(24)}$$

Note that P_{max} should be designed larger than the rated power with a margin of 10%.

B. Parameters of Four-winding Transformers

Table II shows the measured and calculated parameters of the four-winding transformers in Fig. 9. The equivalent values

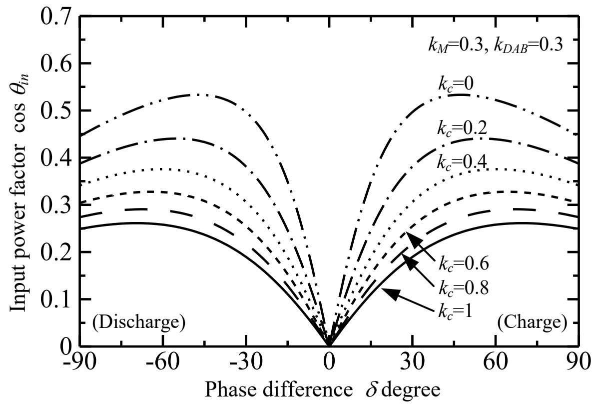

Fig. 8. Theoretical curves of power factor given by (23). Only k_c value is changed from 1 to 0. The other coupling coefficients of k_M and k_{DAB} are fixed value in order to verify effect of reducing k_c.

Table I. Test conditions.

Parameter	Symbol	Value
Input DC voltage	V_{in}	280 V
Output DC voltage	V_{out}	280 V
Rated power	P	1.1 kW
Switching frequency	f_{sw}	84.75 kHz
Dead time	T_{dead}	300 ns
Smoothing capacitors	C_{in} ,C_{out}	2.7 mF
Smoothing inductor	L_{in} ,L_{out}	2 mH
MOSFETs	S_1-S_8	IXYS, IXFN80N60P3

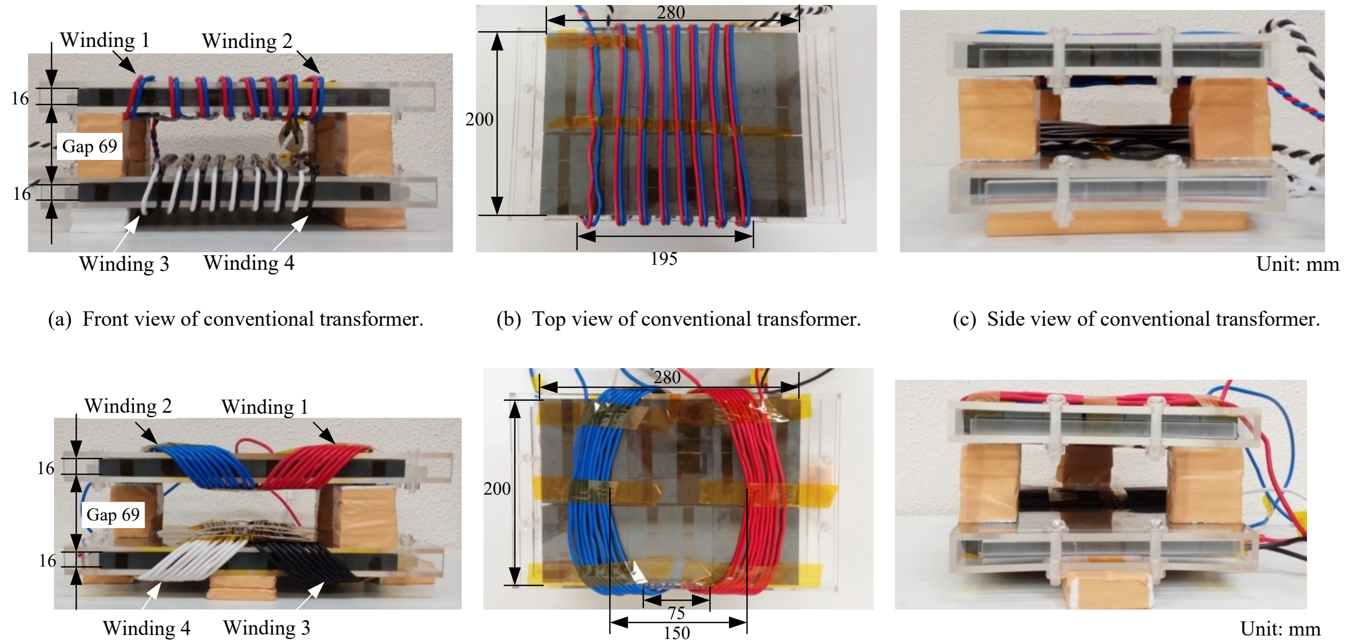

(a) Front view of conventional transformer. (b) Top view of conventional transformer. (c) Side view of conventional transformer.

(d) Front view of proposed transformer. (e) Top view of proposed transformer. (f) Side view of proposed transformer.

Fig. 9. Two prototype four-winding transformers. The outline drawing from (a) to (c) are the conventional transformer whose windings of the primary or secondary side are close to each other. The outline drawing from (d) to (f) are the proposed transformer whose windings of the primary or secondary side are separated to introduce the proposed method.

Table II. Measurement results of inductance and coupling coefficients of conventional transformer and proposed transformer. The matrix elements of $\boldsymbol{L_{Trans}}$ are measured by a LCR meter. According to (9), the parameters L_{DAB}, k_c, k_M and k_{DAB} are averaged from the matrix elements of $\boldsymbol{L_{Trans}}$.

Parameters		**Conventional Transformer**	**Proposed Transformer**
Coils turns	Primary coils	8	9
	Secondary coils	8	9
Inductance matrix $\boldsymbol{L_{Trans}}$ as 4-winding transformer		$\begin{pmatrix} 34.6 & 33.1 & 11.2 & 11.2 \\ 33.1 & 34.6 & 11.1 & 11.1 \\ 11.2 & 11.1 & 35.2 & 33.7 \\ 11.2 & 11.1 & 33.7 & 35.2 \end{pmatrix}$ [μH]	$\begin{pmatrix} 57.6 & 30.2 & 17.3 & 14.5 \\ 30.2 & 59.9 & 15.5 & 18.0 \\ 17.3 & 15.5 & 56.0 & 27.4 \\ 14.5 & 18.0 & 27.4 & 58.1 \end{pmatrix}$ [μH]
Self-inductance L_{DAB}	Measured value	34.9 μH	57.9 μH
Coupling coefficient k_c	Measured value	0.958	0.497
Coupling coefficient k_M	Measured value	0.320	0.304
Coupling coefficient k_{DAB}	Measured value	0.320	0.260
Equivalent primary self-inductance L_p	Measured value	33.9 μH	44.4 μH
	Calculated value	34.2 μH	43.3 μH
Equivalent secondary self-inductance L_s	Measured value	34.5 μH	42.4 μH
	Calculated value	34.2 μH	43.3 μH
Equivalent mutual inductance M	Measured value	11.2 μH	16.4 μH
	Calculated value	11.2 μH	16.3 μH
Equivalent coupling coefficient k_{eq}	Measured value	0.329	0.377
	Calculated value	0.327	0.376
Maximum error of calculated inductances		1.0 %	2.4 %
Error of calculated coupling coefficient		0.7 %	0.2 %

L_p, L_s, M and k_{eq} show both of calculate values and measured values by connecting the windings in parallel. The coupling coefficient k_c of the proposed transformer is 0.497 weaker than k_c of the conventional transformer of 0.958. Consequently, k_{eq} of the proposed transformer improves to 0.377 from 0.329. In addition, the validity of the formulations is also confirmed and all the errors of L_p, L_s, M and k_{eq} is below 2.4%.

Note that k_M and k_{DAB} of the proposed transformer are weaker than the value of the conventional transformer because the distances of the windings are longer. Equation (19) shows that k_{eq} is proportional to the sum of k_M and k_{DAB}. Thus a winding method which only reduce k_c without decreasing k_M and k_{DAB} is required to increase k_{eq}.

C. Operation Waveforms of Proposed System

Fig. 10 shows the operation waveforms at rated load and at light load in the power charging and the discharging operation. The phase difference δ is 90 degree at rated load and 15

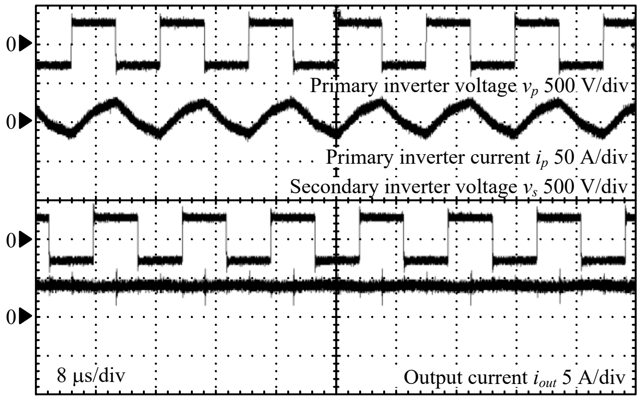

(a) Rated load (1.1 kW) with charging operation.

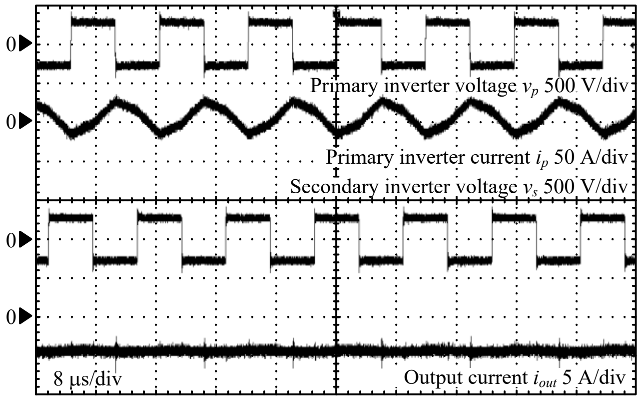

(b) Rated load (1.1 kW) with discharging operation.

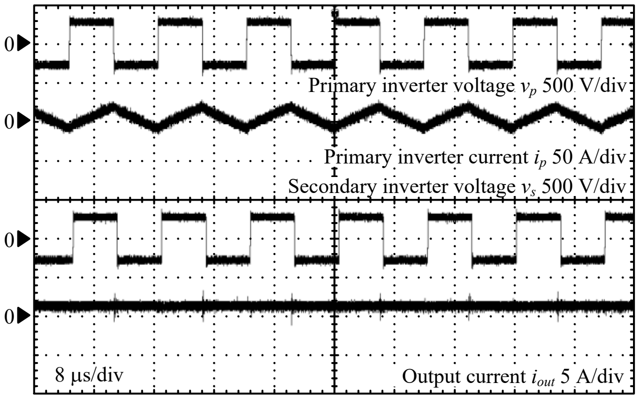

(c) Light load (300 W) with charging operation.

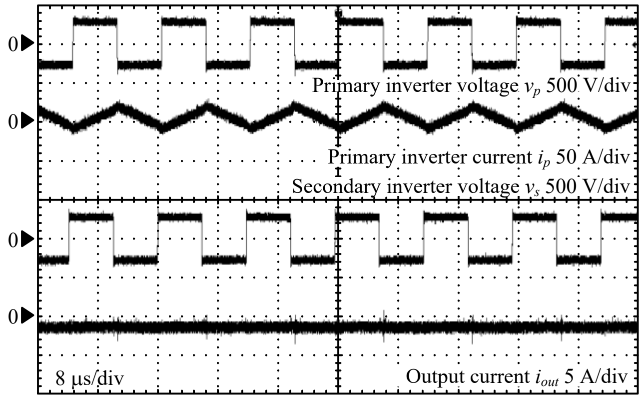

(d) Light load (300W) with discharging operation.

Fig. 10. Operation waveforms of prototype circuit with proposed transformer. The transmission power and the operation mode are changed by the phase difference between the primary-side inverter and the secondary-side inverter output voltage. (a) δ = 90 degree. (b) δ = -90 degree. (c) δ = 15 degree. (b) δ = -15 degree.

degree at light load. At light load, the current is a triangle wave because the reactive current is dominant.

The output DC current i_{out} shows that power transmitting is achieved at the proposed transformer in both of the power charging and the discharging operation.

D. Characteristics of Input Current, Power Factor and Efficiency

Fig. 11 shows characteristics of the primary current I_{p_rms} versus output power P_{out}. Note that the measurement value is plotted in the graph, and the theoretical characteristics are drawn by the solid line or the dotted lines. According to the I_{p_rms} values at P_{out} = 0 W, the excitation current of the proposed transformer reduces by 25% compared with the conventional values.

Fig. 12 shows characteristics of the input power factor cos θ_{in}. The x-axis of Fig. 12 (a) is the phase shift angle δ. The x-axis of Fig. 12 (b) is P_{out}. The measurement value is plotted in the graph, and the theoretical characteristics are drawn by the solid line or the dotted lines. In order to measuring cos θ_{in}, i_p and v_p are detected directly. Note that effect of the detection parts are not taken into account in the calculation process of theoretical cos θ_{in} value.

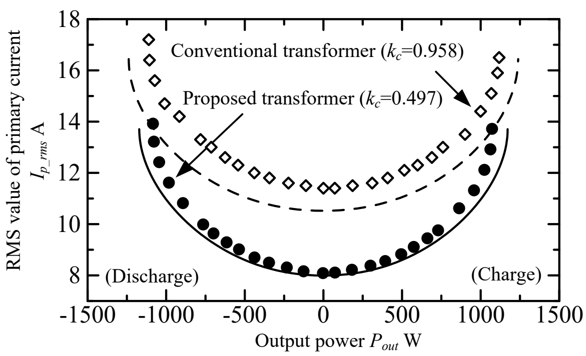

Fig. 11. Characteristics of RMS values of primary-side inverter AC output current. The theoretical characteristics are shown by curves, whereas the plots are measurement values.

The maximum power factor of the proposed transformer is 17% larger than the conventional transformer. Moreover, cos θ_{in} is improved the entire load range. Thus a low-k_c transformer improves the system efficiency owing to the reduction of the reactive current.

Fig. 13 shows the system efficiency versus P_{out}. The system efficiency is improved over the entire P_{out} with the proposed transformer. The maximum efficiency of the proposed transformer is 87.3% at 1.00 kW in the charging operation. The efficiency of the proposed transformer is improved over entire load range compared to the conventional transformer. In particular, the maximum efficiency of the proposed transformer is 90.3 % at 891 W in the discharging operation, which is 3.0% higher than that of the conventional transformer.

V. CONCLUSION

In this paper, a power factor correction method was proposed for the non-resonant IPT system utilizing the dual active bridge converter in order to reduce conduction loss and winding loss. The loose coupling coefficient k_c between two pairs of the primary-side and the secondary-side wires connected in parallel contributed to the power factor correction from the viewpoint of the power supply. Therefore, the low-k_c four-winding transformer improved efficiency because of the strong equivalent coupling coefficient k_{eq} between the primary side and the secondary side.

From the experiment, the maximum power factor of the low-k_c transformer, k_c value of which is 0.497, was improved by 17% compared with the high-k_c transformer because of stronger k_{eq} by 15%. Besides, the maximum efficiency of the low-k_c transformer was improved by 3.0%.

In the future, the proposed method will be introduced to a resonant IPT systems in order to improve efficiency.

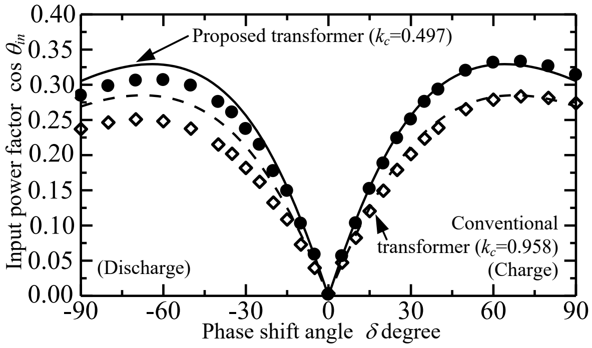

(a) Versus phase shift angle.

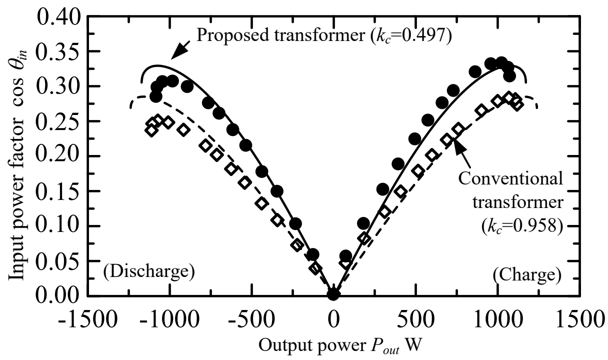

(b) Versus output power of the system.

Fig. 12. Characteristics of power factor. The theoretical characteristics are shown by curves, whereas the plots are measurement values. The power factor cos θ_{in} is measured with the power analyzer (E.E.Corporation, PW6001) and Direct Current Measurement Option (E.E.Corporation, PW9100).

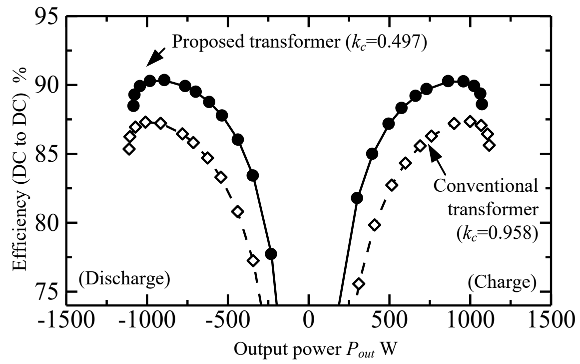

Fig. 13. Efficiency of each four-winding transformer. The plots are measurement values under the conditions of Table I.

REFERENCES

[1] Siqi Li and Chunting Chris Mi: “Wireless Power Transfer for Electric Vehicle Applications”, IEEE Trans. PE, Vol.3, No.1 pp. 4-17J. Clerk Maxwell, A Treatise on Electricity and Magnetism, 3rd ed., vol. 2. Oxford: Clarendon, 1892, pp.68-73.(2015)

[2] Su Y. Choi, Beom W. Gu, Seog Y. Jeong and Chun T. Rim: “Advances in Wireless Power Transfer Systems for Roadway-Powered Electric Vehicles”, IEEE Trans. PE, Vol.3, No.1 pp.18 - 36 (2015)K. Elissa, “Title of paper if known,” unpublished.

[3] Fei Lu, Hua Zhang, Heath Hofmann and Chunting Chris Mi: “An Inductive and Capacitive Combined Wireless Power Transfer System With LC-Compensated Topology”, IEEE Trans. PE, Vol.24, No.4 pp.1115-1124 (2009)

[4] Tsutomu Mizuno, Takuto Ueda, Shintaro Yachi, Ryuhei Ohtomo and Yoshihito Goto: "Dependence of Efficiency on Wire Type and Number of Strands of Litz Wire for Wireless Power Transfer of Magnetic Resonant Coupling", IEEJ Journal of Industry Applications, Vol. 3, No. 1, pp. 35-40 (2014)

[5] Hiroki Ishida, Hiroto Furukawa and Tomoaki Kyoden: "Development of Design Methodology for 60 Hz Wireless Power Transmission System", IEEJ Journal of Industry Applications, Vol. 5, No. 6, pp. 429-438 (2016)

[6] Daisuke Shimode, Toshiaki Murai and Shunsuke Fujiwara: "A Study of Structure of Inductive Power Transfer Coil for Railway Vehicles", IEEJ Journal of Industry Applications, Vol. 4, No. 5, pp. 550-558 (2015)

[7] H. Sakamoto, K. Harada, S. Washimiya, K. Takehara and Y. Matsuo: "Large Air-Gap Coupler for Inductive Charger", IEEE TRANSACTIONS ON MAGNETICS, Vol. 35, No. 5, pp. 3526-3528 (1999)

[8] Roman Bosshard, Johann Walter Kolar, Jonas Mühlethaler, Ivica Stevanovi´c, Bernhard Wunsch, and Francisco Canales: " Modeling and η-α-Pareto Optimization of Inductive Power Transfer Coils for Electric Vehicles", IEEE Trans. PE, Vol.3, No.1 pp.50-64 (2015)

[9] Keisuke Kusaka and Jun-ichi Itoh: “Non-resonant Inductive Power Transfer System based on the Principle of Dual Active Bridge Converter”, IEEJ Trans. I.A., Vol. 136, No.2, pp. 189-197(2015)

[10] Mustansir H. Kheraluwala, Randal W. Gascoigne, Deepakraj M. Divan, and Eric D. Baumann: “Performance Characterization of a High-Power Dual Active Bridge dc-to-dc Converter”, IEEE Trans. IA, Vol.28, No.6 pp.1294-1301 (1992)

[11] Keizo Inagaki, Masaru Higaki, Yoshiaki Matsui and Kentaro Kurita: “Digital protection method for power transformers based on an equivalent circuit composed of inverse inductance”, IEEE Trans. PD, Vol.3, No.4 pp. 1501-1510 (1988)